THE JOURNAL OF PHYSICAL CHEMISTRY A

ARTICLE

pubs.acs.org/JPCA

Density Functional Theory Study of Pyrophyllite and M-Montmorillonites (M = Li, Na, K, Mg, and Ca): Role of Dispersion Interactions

Vamsee K. Voora,[†,‡] W. A. Al-Saidi,[†,§] and Kenneth D. Jordan*[,†,‡]

[†]Department of Chemistry and Center for Molecular and Materials Simulations, University of Pittsburgh, Pittsburgh, Pennsylvania 15260, United States

[‡]National Energy Technology Laboratory, 626 Cochrans Mill Road, Pittsburgh, Pennsylvania 15236, United States

[§]Department of Chemical and Petroleum Engineering, University of Pittsburgh, Pittsburgh, Pennsylvania 15261, United States

ABSTRACT: The stacking parameters, lattice constants, bond lengths, and bulk moduli of pyrophyllite and montmorillonites (MMTs), with alkali and alkali earth metal ions, are investigated using density functional theory with and without dispersion corrections. For pyrophyllite, it is found that the inclusion of the dispersion corrections significantly improves the agreement of the calculated values of the lattice parameters and bulk modulus with the experimental values. For the MMTs, the calculations predict that the interlayer spacing varies approximately linearly with the cation radius. The inclusion of dispersion corrections leads to sizable shifts of the interlayer spacings to shorter values. In Li-MMT, compaction of the interlayer distance triggers migration of the Li ion into the tetrahedral sheet and close coordination with basal oxygen atoms. Analysis of electron density distributions shows that the isomorphic octahedral Al^{3+}/Mg^{2+} substitution in MMT causes an increase of electron density on the basal oxygen atoms of the tetrahedral sheets.

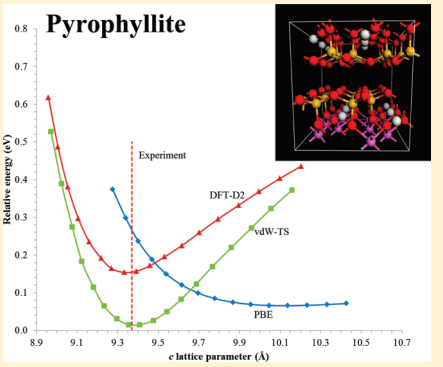

1. INTRODUCTION

Clay minerals are an important class of layered phyllosilicate materials with many useful physicochemical properties, including swelling, adsorption, surface acidity, catalysis, and ion-exchange.[1−3] The properties of clays can vary widely, depending on ion substitutions.[4,5] The expansive nature of clay materials enables them to form polymer composites and other intercalates[6] with improved mechanical stress, heat resistance, and other properties,[7−11] and also renders them useful in oil drilling, where they are mixed with water to cool and to lubricate drill bits.[12] They are also used as liners for disposal of nuclear wastes[13,14] and for dams and lakes.[15] Recently, clay materials have been proposed for use in CO_2 sequestration.[16] Many of the unique characteristics of clays stem from their swelling upon intercalation,[17] which can sometimes be undesirable as it may destabilize engineered structures.[18] A key factor that influences the extent of swelling of clays is the presence of exchangeable cations present in the interlayers.[19−33]

Several force fields, including CLAYFF,[34] phyllosilicate force field (PFF),[35] MS-Q,[36] and others,[37−41] have been developed for modeling clay materials. Zeolite-based force fields have also been used in modeling clays.[42−44] Force-field approaches are very attractive in terms of computational cost, however, they are often unreliable when used for conditions and systems that differ significantly from those for which they were parametrized.[35,45] Electronic structure approaches, in particular, density functional theory (DFT), while more computationally demanding, do not suffer from such transferability problems. Sainz-Diaz and co-workers have used DFT to study octahedral- and tetrahedral-cationic substitutions on pyrophyllite, smectites, and illites.[46−48] DFT has also been used to study how the equilibrium structure of clays depends on the choice of the interlayer cation.[49,50]

Clays are layered materials, with the layers being stacked and held together by electrostatic, polarization, and dispersion interactions. As in other layered materials, such as graphite, *h*-boron nitrides, and metal-intercalated graphene, dispersion interactions are expected to be important, especially for describing interactions along the stacking direction.[51,52] Standard DFT methods fail to describe long-range dispersion interactions, and hence, DFT calculations usually overestimate the lattice parameters along the stacking direction for such materials.[51,52] Several approaches have been proposed for correcting DFT for dispersion, including the DFT-D2 and DFT-D3 methods of Grimme and co-workers,[53−55] van der Waals density functionals (vdW-DF) of Lundqvist, Langreth, and co-workers,[56−58] the dispersion-corrected atom-centered pseudopotential method of Roethlisberger and co-workers,[59,60] and the vdW-TS method of Tkatchenko and Scheffler.[61] The DFT-D2 method was recently applied to the clay system kaolinite.[36]

Special Issue: David W. Pratt Festschrift

Received: February 8, 2011
Revised: April 3, 2011
Published: April 26, 2011

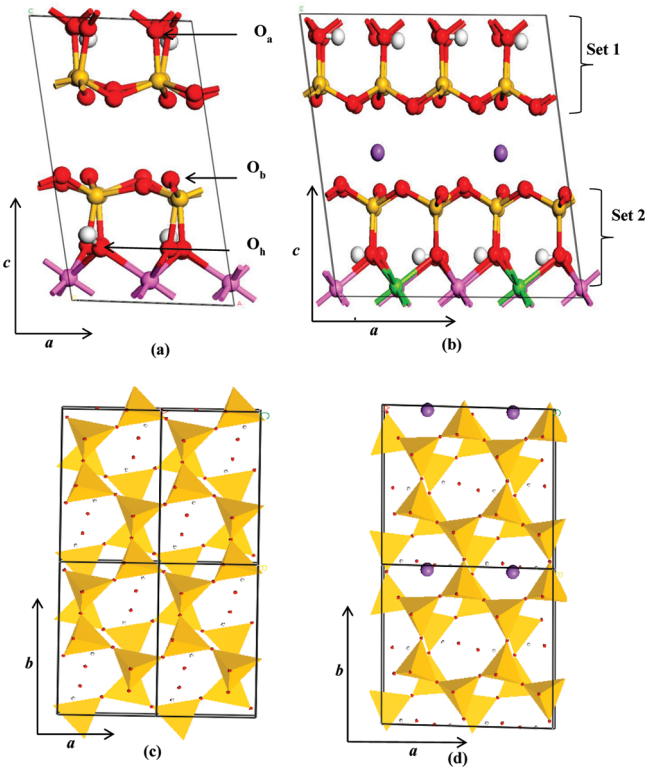

Figure 1. Supercells used for the pyrophyllite and MMT simulations: (a) 1 × 1 × 1 unit cell of pyrophyllite; (b) 2 × 1 × 1 unit cell for MMT with Mg substituted for Al, as shown. The cations are situated in the interlayer: (c) projection along the *ab* plane for pyrophyllite and (d) projection along the *ab* plane for MMT. The six-membered rings formed by silicon-occupied tetrahedra are called ditrigonal rings and enclose a cavity. The Na cations can be seen underneath and above the ditrigonal cavity. For (c) and (d), the cations in the octahedra are removed for the sake of clarity. The black solid lines indicate the unit cell, and the color coding for the atoms is H (white), O (red), Mg (green), Al (pink), Si (gold), and cation (purple). O_a, O_b, and O_h denote apical, basal, and hydroxyl oxygen atoms, respectively.

In this paper, we apply the DFT-D2 and vdW-TS methods, which have little computational overhead compared to nondispersion corrected DFT methods, to dioctahedral 2:1 phyllosilicates, which have one octahedral sheet sandwiched between two tetrahedral sheets. The tetrahedral sheets are formed by linking tetrahedra of oxygen atoms through three shared oxygen (basal oxygen, O_b) atoms in each tetrahedra. Hydroxyl groups together with the free unlinked fourth oxygen (apical oxygen, O_a) atom from the tetrahedra form the octahedral sheets. The most common ions occupying the octahedra are Al^{3+}, Mg^{2+} and Fe^{3+}, and the most common ions occupying the tetrahedra are Si^{4+} and Al^{3+}. In dioctahedral 2:1 phyllosilicates, only two-thirds of the octahedra are occupied. If the vacancies are *cis* with respect to the hydroxyl groups, then the phyllosilicate is designated *cis*-vacant, otherwise, it is *trans*-vacant. Minisini et al. and Tunega et al. have shown that the energy difference between the two isomers is minor, and whether the vacancies are *cis* or *trans* groups mainly affects the orientation of the hydroxyl groups.[62,63] In our studies, we focus on the *trans*-isomer, which is more prevalent in nature.

The 2:1 dioctahedral phyllosilicate with only silicon ions occupying the tetrahedra and only aluminum ions occupying the octahedra is known as pyrophyllite. The 2:1 layers of pyrophyllite are held together by weak van der Waals forces in addition to the electrostatic forces. Naturally occurring clays have many different substitutions and can have different intercalated cations. Some of the silicon ions belonging to the tetrahedra can be substituted isomorphically by Al^{3+}, and the octahedral aluminum ions can be substituted by Mg^{2+} or Fe^{3+}. If the Al atoms of pyrophyllite are substituted by other atoms leading to charged layers, the clay systems are then known as dioctahedral smectites or montmorillonites (MMTs). In this study, only $Al^{3+} \rightarrow Mg^{2+}$ substitution is considered. This substitution results in negatively charged layers, with the negative charge being counterbalanced by cations located in the interlayer region. This can be seen from Figure 1, which displays the supercells used in the simulations. The counter-balancing cations are generally alkali or alkaline-earth ions. The MMTs are then named after the counterion. For example, for Na^+ counterions, the clay is known as Na-MMT. The interlayer cations are readily hydrated and, hence, play a major role in the swelling properties of clays.[19−33]

Table 1. Average Bond Lengths (Å) in Pyrophyllite Obtained from Experiment and Various Theoretical Methods

bond type[a]	expt[b]	CLAYFF[c]	PBE[d]	DFT-D2[d]	vdW-TS[d]
HO_h	0.978	1.106(2)	0.970	0.971	0.969
SiO_b	1.615	1.580(33)	1.628	1.627	1.626
SiO_a	1.614	1.578(36)	1.652	1.650	1.648
AlO_h	1.897	1.959(98)	1.906	1.898	1.896
AlO_a	1.927	2.056(159)	1.941	1.935	1.933

[a] O_h represents a hydroxyl oxygen, O_b represents a basal oxygen, and O_a represents the apex oxygen of the SiO_4 tetrahedral. [b] Ref 76. [c] Ref 34. The CLAYFF results are from NPT MD simulations at T = 300 K and P = 0.1 MPa, with statistical errors shown between the parentheses. [d] Present work.

2. THEORETICAL DETAILS

2.1. Methodology and Computational Details. The DFT calculations were carried out using the Vienna ab initio simulation package (VASP)[64,65] using Blochl's projector augmented wave (PAW) technique.[66] The gradient-corrected PBE functional[67] was used in conjunction with the DFT-D2[54] and vdW-TS procedures described below for including long-range two-body dispersion corrections.[61] The DFT-D2 method is available in VASP 5.2.[68] Additionally, we have implemented the vdW-TS scheme in a local copy of VASP 5.2[69] following the formalism reported in ref 61.

We restrict our studies to pyrophyllite and to the 2:1 dioctahedral smectites (MMTs). A 1 × 1 × 1 unit cell with the $[(Al_4O_8(OH)_4)(Si_8O_{12})]$ repeating unit was used in the case of pyrophyllite. For the MMTs, a 2 × 1 × 1 supercell with one isomorphic octahedral Al^{3+}/Mg^{2+} substitution per unit cell was employed. This corresponds to one unit charge substitution for every $O_{20}(OH)_4$ unit. The negative charge introduced by this substitution is compensated by the introduction of a metal cation between the layers. Li, Na, K, Mg, and Ca interlayer cations were considered. In the present study, the interlayer cations are not hydrated. The impact of hydration on the properties of the clays will be considered in the future work. Thus, M-MMT supercell with M as the cation has formula $M_x[(MgAl_3O_8(OH)_4)(Si_8O_{12})]_2$, where x = 2 for alkali cations (Li, Na, K) and x = 1

Table 2. Equilibrium Lattice Parameters, a, b, c, α, β, and γ, Equilibrium Volume V_0, Bulk Modulus B_0, and the Pressure Derivative of the Bulk Molecules, B_0' for Pyrophyllite

method	a (Å)	b (Å)	c (Å)	α (deg)	β (deg)	γ (deg)	V_0 (Å^3)	B_0 (GPa)	B_0'
expt[a]	5.160(2)	8.966(3)	9.347e(6)	91.18(4)	100.46(4)	89.64(3)	425.157	37(3)[h]	10(1) [h]
expt[b]	5.161(1)	8.958(2)	9.351(2)	91.03(2)	100.37(2)	89.75(2)	425.187		
PBE[i]	5.224	9.076	10.138	90.85	100.06	89.7	471.81	6	19
vdW-TS[i]	5.187	8.997	9.408	90.67	100.36	89.95	429.57	41	12
DFT-D2[i]	5.177	8.994	9.332	90.88	100.50	89.82	428.84	38	11
PFF[c]	5.17	8.97	9.36	90.65	101.18	90.06	426		
CLAYFF[d]	5.192(34)	9.021(61)	9.459(163)	91.38(87)	98.97(190)	89.81(47)			
PW91[e]	5.260	9.119	10.106	90.07	101.60	89.79	474.833		
PBE[f]	5.15	8.98	9.21	88.96	99.80	90.0	420.23		
PBE[g]	5.17	9.00	9.25	91.09	100.81	89.89			
	5.12	8.91	9.52	90.64	100.56	89.67			

[a] Ref 76. [b] Ref 79. [c] Ref 35. [d] Ref 34. [e] Ref 77. [f] Ref 46. [g] Ref 78. The first set of results was obtained using SIESTA and the second set using CASTEP. [h] Ref 80. [i] Present work.

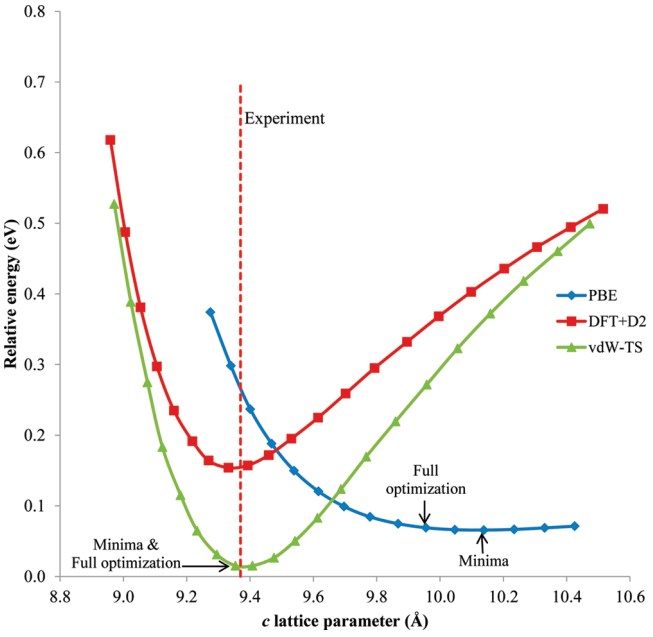

Figure 2. Energy vs c lattice constant for pyrophyllite. The vertical dotted line indicates the experimental value of the lattice constant. The choice of the zero of energy for each approach is arbitrary.

for alkaline-earth cations (Mg, Ca). Symmetry was turned off in the optimizations of the Li-, Na-, and K-MMTs to permit the two cations in the unit cell to optimize independently.

For K and Ca, the valence and the semicore 3s and 3p electrons were treated explicitly. For pyrophyllite, a 2 × 2 × 1 Monkhorst-Pack[70] k-point grid was used to sample the Brillouin zone, whereas for the MMT systems, the calculations were restricted to the Γ point because of the large size of the unit cell. A plane-wave energy cutoff of 1000 eV was employed in the calculations on both the pyrophyllite and the MMT systems; the use of this large energy cutoff ensures that the Pulay stress[71] is small during the lattice optimization. We used a convergence criteria of 0.01 meV for total energy and 10 meV/Å for total force. Tests were also performed to make sure the calculations are well converged with respect to the k-point grid. Specifically for pyrophyllite, calculations were carried out with both 2 × 2 × 1 and 4 × 4 × 2 Monkhorst-Pack k-point grids; and for a subset of the MMTs, calculations were carried out using a 2 × 2 × 1 k-point grid, as well as using the Γ point only. In both cases, the lattice constants are changed by less than 0.005 Å upon adoption of the larger k-point grid.

For both the pyrophyllite and the MMT systems, potential energy curves were mapped out along the crystallographic c-direction by relaxing the atomic positions and the remaining lattice parameters for a series of 10−15 c lattice vectors spanning 1.0−1.5 Å around the potential energy minimum. This approach is similar to that used by Berghout et al.[50] The minima of the potential energy curves correspond to the equilibrium values of the c lattice parameters. Due to the shallowness of the potential energy curves obtained with the PBE functional without dispersion corrections, determination of the c lattice parameters from full optimization rather than the grid-based approach adopted in this study would require the use of even tighter convergence criteria and a higher energy plane-wave cutoff.

The bulk modulus of a clay system under a triaxial pressure can be extracted using the energies from the series of constant volume optimizations described above. This is done by fitting the energies to the Birch-Murnhaghan equation of state:[72]

$$E(V) = E_0 + \frac{B_0 V}{B_0'}\left(\frac{(V_0/V)^{B_0'}}{B_0'} + 1\right) - \frac{B_0 V_0}{B_0' - 1} \qquad (1)$$

where B_0 is the bulk modulus, B_0' is the pressure derivative of bulk modulus, and E_0 and V_0 are the equilibrium energy and volume, respectively.

The partitioning of the electron charge density into contributions from individual atoms can provide insights into the changes that occur upon chemical substitution. In this work, this is accomplished by use of Bader charge analysis[73] using the approach of Henkelman et al.[74]

2.2. DFT-D2 and vdW-TS. The dispersion-corrected density functional energies are given by the sum of the Kohn−Sham energy (E_{DFT}) and a correction term (E_{disp}): $E_{DFT+disp} = E_{DFT} + E_{disp}$. In both the DFT-D2 and the vdW-TS schemes, the dispersion correction E_{disp} is the sum of damped atom−atom C_6^{AB}/R^{-6} terms where R is the atom−atom distance, and A and B denote the atom types. The damping function is introduced to avoid divergence at small R and double counting. In both approaches,

Table 3. Bader Charges for Pyrophyllite at the PBE, DFT-D2, and vdW-TS Optimized Structures

	atom type[a]										
method	H_1	H_2	Al	O_{a1}	O_{a2}	O_{b1}	O_{b2}	O_{h1}	O_{h2}	Si_1	Si_2
PBE	0.601	0.609	2.490	−1.614	−1.616	−1.595	−1.595	−1.424	−1.431	3.173	3.174
DFT-D2	0.600	0.604	2.488	−1.615	−1.614	−1.594	−1.594	−1.423	−1.426	3.173	3.173
vdW-TS	0.603	0.606	2.493	−1.619	−1.620	−1.597	−1.595	−1.427	−1.431	3.179	3.179

[a] The 1 and 2 in the subscripts refer respectively to sets 1 and 2 in Figure 1.

Table 4. Structural Parameters, Volumes, and Bulk Moduli of a Series of Montmorillonites

	method	a (Å)	b (Å)	c (Å)	d_{001}	α (°)	β (°)	γ (°)	V_0 (Å^3)	B_0 (GPa)	B_0'
Li-MMT	BP[a]	10.26	8.88	10.90		89.96	99.11	89.94			
	PBE	10.51	9.09	9.82	9.70	83.01	95.53	90.12	925.96	23.61	12.56
	DFT-D2	10.35	8.98	9.24	9.06	80.70	96.30	89.80			
	vdW-TS	10.38	9.03	9.45	9.29	81.54	96.49	89.80	867.51	61.67	15.86
	expt				9.6,[c] 9.6[d]						
Na-MMT	BP[a]	10.29	8.95	10.53		90.22	97.58	89.97			
	PW92[b]	10.48	9.08	10.36		89.60	98.70	90.00	974.32	13.00	
	PBE	10.50	9.09	10.08	9.83	98.69	99.27	90.07	943.46	22.93	14.55
	DFT-D2	10.45	9.07	9.57	9.32	99.37	99.18	90.14	881.06	46.91	14.72
	vdW-TS	10.42	9.04	9.68	9.47	97.05	99.52	90.09	888.01	46.38	11.00
	expt				9.6,[c] 9.6[d]						
K-MMT	BP[a]	10.24	8.91	10.80		89.98	96.95	90.92			
	PBE	10.53	9.08	10.49	10.28	90.03	101.53	90.00	985.12	24.03	19.13
	DFT-D2	10.45	9.03	10.04	9.81	90.02	102.31	90.00	928.68	41.95	12.47
	vdW-TS	10.44	9.06	10.07	9.88	90.01	101.01	90.00	931.52	47.04	8.95
	expt				10.0,[c] 10.0[d]						
Mg-MMT	BP[a]	10.33	8.89	10.19		89.84	97.85	89.91			
	PW92[b]	10.50	9.03	10.07		90.70	99.20	89.70	942.83	22.00	
	PBE	10.51	9.08	9.75	9.55	80.81	97.12	89.93	909.08	36.42	10.49
	DFT-D2	10.39	9.02	9.30	9.12	80.60	96.47	89.75	856.60	59.05	8.66
	vdW-TS	10.40	9.04	9.39	9.19	80.44	96.42	89.78	859.26	58.19	11.91
	expt				9.6,[c] 10.0[d]						
Ca-MMT	BP[a]	10.28	8.96	10.55		89.99	99.50	89.96			
	PW92[b]	10.48	9.03	10.05		90.00	99.30	90.00	940.12	25.00	
	PBE	10.53	9.12	10.06	9.71	100.25	101.30	90.04	929.51	35.06	11.68
	DFT-D2	10.45	9.08	9.60	9.33	99.38	99.78	90.09	886.31	45.96	11.06
	vdW-TS	10.44	9.08	9.62	9.33	99.59	99.97	90.08	887.13	54.70	5.46
	expt				9.6,[c] 10.0[d]						

[a] Ref 49. [b] Ref 50. [c] Ref 33. [d] Ref 30.

the C_6^{AB} coefficients for interaction between different atom species are defined in terms of C_6^{AA} and C_6^{BB} coefficients by use of combination rules. The main drawback of the DFT-D2 approach is that the C_6 coefficients are insensitive to the chemical environment. This problem is partly alleviated in the vdW-TS approach where the effective C_6^{AA} coefficients are scaled according to the ratio of the Hirschfield volumes of the atom-in-molecules to those of the free atoms.[75] More details can be found in ref 61.

3. RESULTS AND DISCUSSIONS

3.1. Pyrophyllite. Table 1 reports the average HO_h, SiO_b, SiO_a, AlO_h and AlO_a bond lengths within the layers of the optimized pyrophyllite structure. Here O_h represents a hydroxyl oxygen, O_b represents a basal oxygen, and O_a represents an apex oxygen of a silicate tetrahedron in the tetrahedral sheet. Results are reported for PBE calculations with and without dispersion corrections. For comparison, experimental results are included.[76] The present PBE values for the bond lengths are in good agreement with the PW91 and PBE calculations of Refson et al.[77] and Craig et al.,[78] respectively. Inclusion of dispersion interactions has little effect on the bond lengths within the layers of pyrophyllite.

Table 2 summarizes the structural parameters of the optimized pyrophyllite unit cell. As expected, inclusion of long-range dispersion corrections in the DFT calculations has little effect on the lattice angles or the in-plane lattice parameters, a and b. Our calculated values of these parameters are in good agreement with those from experiment and from previous calculations.[46,77,78] However, our calculations give a value of the c

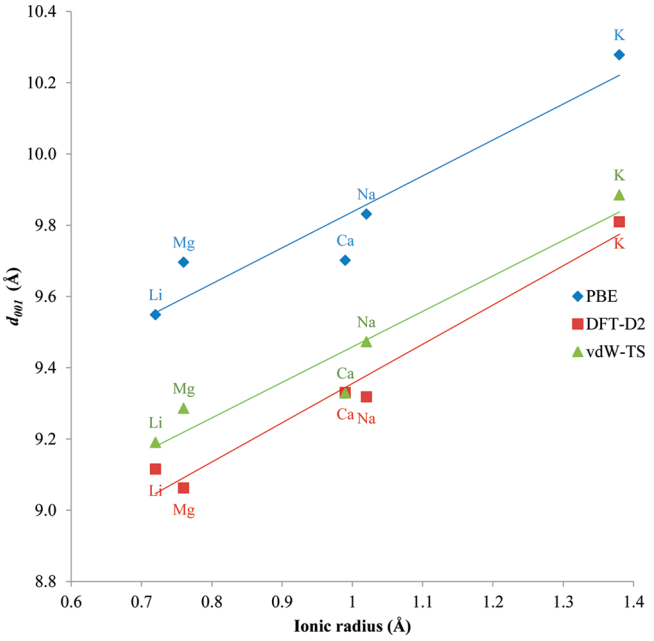

Figure 3. The interlayer separation, d_{001} vs the ionic radius of the counterions of the MMT systems.

parameter ~0.5−0.7 Å larger than that obtained previously[46,78] using the same (PBE) functional. The smaller value of the *c* lattice parameter obtained in these earlier studies may be a consequence of their use of small, atom-centered, basis sets, causing appreciable basis-set superposition error. It is also possible that the convergence thresholds used in refs 46 and 78 were not sufficiently tight to yield well converged values of the *c* lattice constant.

The value of the *c* lattice constant obtained in our optimization with the PBE functional is about 0.79 Å larger than the experimental value, which is indicative of missing dispersion interactions. Upon inclusion of dispersion corrections using the DFT-D2 and vdW-TS methods, the *c* lattice constant is reduced to 9.3 and 9.4 Å, respectively, in excellent agreement with the experimental value of 9.35 Å.[76,79] Figure 2 reports the potential energy curves of pyrophyllite along the stacking direction calculated using PBE, DFT-D2, and vdW-TS methods. As noted above, with the PBE functional, the potential energy curve along the *c* direction is extremely flat. When dispersion corrections are included, the potential energy curve becomes much deeper and the value of the *c* parameter corresponding to the potential energy minimum decreases by about 0.8 Å.

Using the Birch-Murnhaghan equation of state, the bulk modulus, B_0, and pressure derivative of the bulk modulus, B_0', were extracted from each of the calculated potential energy curves depicted in Figure 2. Table 2 summarizes the results. The calculations with the PBE functional severely underestimate B_0 and overestimate B_0' due to the shallowness of the potential energy curve. In contrast, the DFT-D2 and vdW-TS values for the bulk modulus of pyrophyllite are 38 and 41 GPa, respectively, which are in good agreement with experimental value of 37 GPa.[80] The B_0' values obtained with the dispersion-corrected DFT methods are also in good agreement with the experimental value. These results demonstrate that both the DFT-D2 and vdW-TS procedures provide superior description of the properties of pyrophyllite that depend on the interlayer spacing than do DFT functionals without long-range dispersion corrections.

Table 3 reports the atomic charges of pyrophyllite obtained from Bader analysis of the electronic charge densities for the PBE, DFT-D2, and vdW-TS optimized structures. As expected, all three sets of calculations give essentially the same atomic charges. The atomic charges of the pyrophyllite system will constitute the reference values against which those of the substituted clays will be compared.

3.2. Montmorillonites. The inhomogeneity and stacking disorder in naturally occurring substituted clay particles precludes single-crystal diffraction studies, and, as a result, only powder X-ray diffraction data[30,33] exist for these systems. In the absence of accurate experimental structural data for such heterogeneous clays, computational results are especially useful for understanding the effects of the substitution on the stacking parameter and other properties. As mentioned above, substitution of Al^{3+} ions by Mg^{2+} ions leads to a net negative charge on the clay layers, which is compensated by the presence of interlayer cations. This introduces additional electrostatic interactions that can impact the properties of interest.

Table 4 summarizes the lattice parameters and the B_0 and B_0' values of five MMTs computed using the PBE, DFT-D2, and vdW-TS methods. For comparison, the basal spacing, d_{001}, determined from powder diffraction studies,[30,33] as well as the lattice parameters from DFT studies of Chaterjee et al.[49] and Berghout et al.[50] are also included. The former authors used the Becke-Perdew (BP) functional[81] to characterize all the MMT systems studied in this paper, while the latter authors used the PW92[82] functional to characterize the Na-, Mg-, and Ca-MMT systems. In most cases, our PBE calculations give appreciably smaller values of the *c* parameter and appreciably different values of the α angle than obtained in the earlier DFT studies. Again, these differences are likely due to our use of a higher plane-wave cutoff energy and an optimization strategy that is effective at dealing with flat potentials.

The variation of the calculated interlayer spacing, d_{001}, with the ionic radius[83] of the interlayer ion, is shown in Figure 3. The correlation between d_{001} and ionic radius has been examined previously for other clay systems.[48] As seen from this figure, the calculated d_{001} values vary approximately linearly with the ionic radius of the ion for all three sets of DFT calculations. On the other hand, the experimental d_{001} values fail to correlate well with the ionic radii of the counterions. We believe that this disagreement mainly reflects the large uncertainties in the experimental d_{001} values. For example, the experimental measurements give the same d_{001} values for Li-MNT and Na-MMT, as well as for Mg-MMT and Ca-MMT (Table 4), which seems highly unlikely. Among other factors, the experimental samples were prepared by dehydrating humidity-exposed clays, which may have led to hysteresis effects, whereby the most stable dehydrated structures might not have been reached.[84,85]

The α and β lattice angles describe how much the bottom tetrahedral surface of one layer is displaced with respect to the top surface of the next layer. For the ideal case of an orthorhombic unit cell, all three lattice angles would be 90°, and consecutive clay layers would be displaced halfway relative to one another. Due to the distorted tetrahedra of pyrophyllite and the MMTs the lattice angles deviate from 90°, with the deviation being greater for β, which has a value of ~100° in the systems considered here (Figure 1). This arrangement of

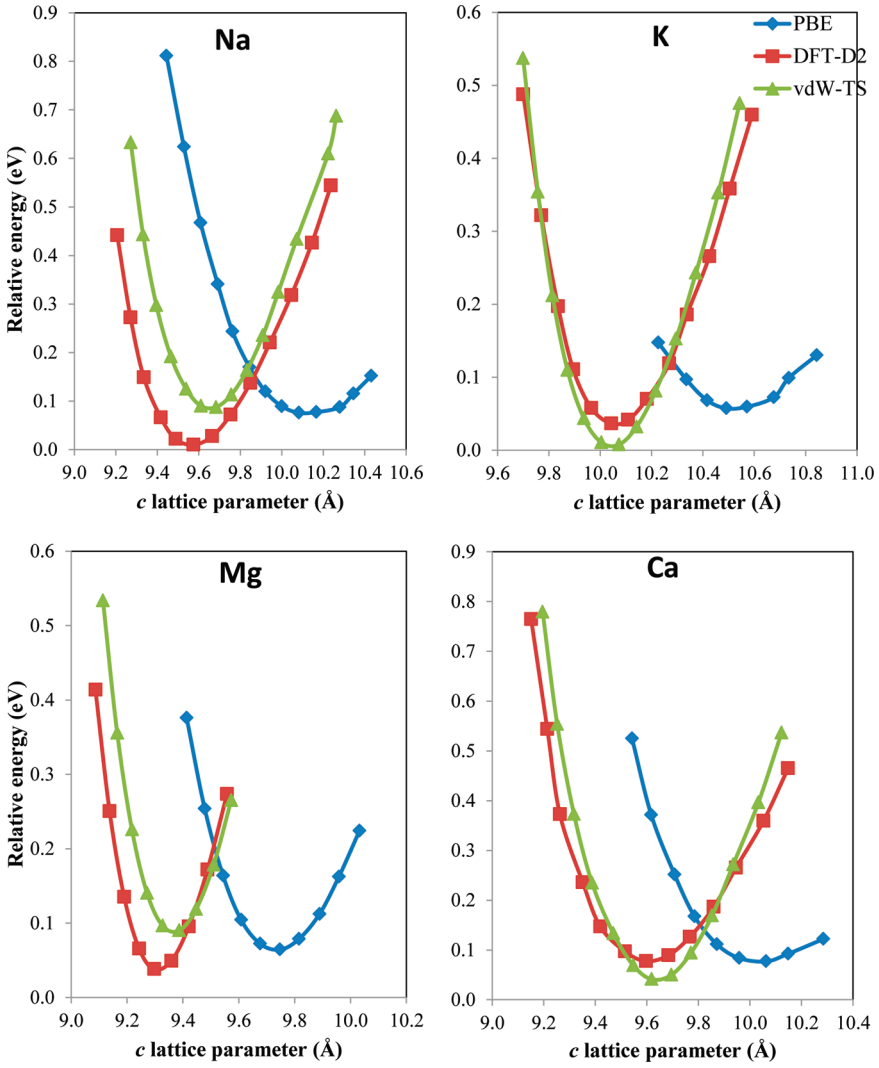

Figure 4. Energy vs *c* lattice constant for the Na-, K-, Mg-, and Ca-MMT systems.

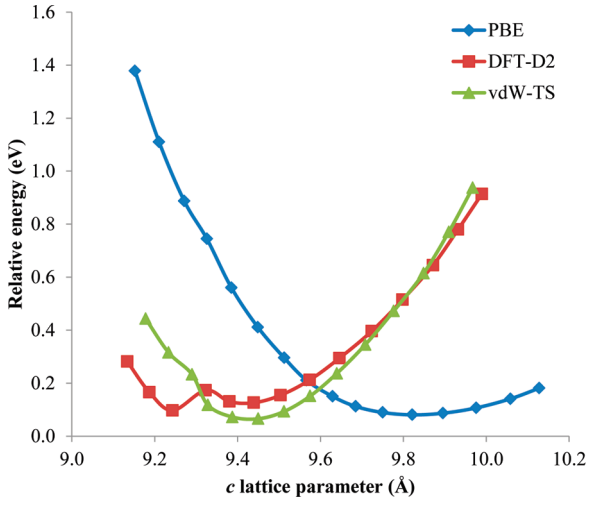

Figure 5. Potential energy curves for Li-MMT. A double minimum is evident in the DFT-D2 curve.

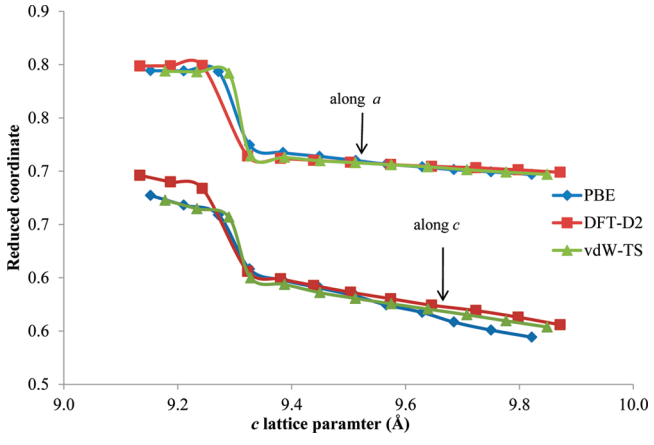

Figure 6. Position of Li^+ cation in the unit cell as a function of the *c* lattice parameter. The reduced coordinates along lattice vectors *a* and *c* are shown.

the layers reduces the electrostatic repulsions between the oxygen ions in adjacent layers.

The potential energy curves for the expansion of the M-MMTs along the *c* lattice direction are reported in Figure 4 for M = Na, K, Mg, and Ca and in Figure 5 for M = Li. As for pyrophyllite, the

dx.doi.org/10.1021/jp201277f |*J. Phys. Chem. A* 2011, 115, 9695–9703

potential energy curves obtained with the functional are shallower than those obtained with the DFT-D2 and vdW-TS methods. However, for the MMTs the potentials are less shallow than those of pyrophyllite (comparing the results for the same method). This is due to the additional electrostatic interaction between the counterions and the negatively charged layers.

For Li-MMT, the interlayer potential energy curve from the DFT-D2 calculations displays two minima, differing primarily in the positions of the intercalated Li cation. To gain additional insight into the factors responsible for this, we report in Figure 6 the position of the Li cation along *a* and *c* directions as a function of the *c* lattice parameter. From this figure it is seen that for all three DFT methods there is a "jump" in the position of the Li^+ ion along both the *a* and *c* directions at $c \sim 9.3$ Å. The short-distance minimum found in the DFT-D2 calculations is driven by the hopping of the Li cation from a position between the clay layers (Figure 7b) into the ditrigonal cavity (Figure 7a). For the DFT-D2 method, the structure with $c \sim 9.2$ Å is about 0.05 eV more stable than that with $c \sim 9.4$ Å, with a negligible barrier between two structures. For the vdW-TS method, the energy is about 0.3 eV lower at $c \sim 9.4$ Å than at 9.2 Å. It is well established that, due to their small radii, Li^+ cations can sit in various cavities of the clay system.[86,87] Thus, the results of the DFT-D2 calculations may, in fact, be more faithfully reproducing the experimental situation. One reservation should be taken into account is that simulations are performed for idealized conditions and without water in the interlayer space.

Our calculations locate the smaller cations, that is, Li^+, Mg^{2+}, and Ca^{2+}, preferentially near one surface, whereas the larger Na^+ and K^+ ions are predicted to be located close to the middle of the interlayer region. In the PW92 calculations of Berghout et al.,[50] the small Mg^{2+} and Ca^{2+} cations, were found to be located near a surface, consistent with our results. In the case of Li-MMT, PBE calculations without the dispersion corrections locate the Li^+ ions in the middle of the interlayer, while the dispersion-corrected DFT calculations bring the Li^+ ions near the surface (and, as discussed above, with DFT-D2, there is a slight preference for the Li^+ ions to move into the ditrigonal cavity for shorter *c* lattice constant). For the other interlayer cations, the locations of the ions were not appreciably altered by the inclusion of dispersion corrections in the calculations. Table 5 summarizes the changes in the atomic charges in going from pyrophyllite to the various M-MMTs. It is seen that for all systems considered, the net charge on the interlayer cations is ~+1.7 (counting both counter ions in the supercell in the case of the alkali cations). This charge is largely counter-balanced by a buildup of about 1.6 electrons at the (Al → Mg) substitution sites (i.e., Al ions with charge ~+2.5 are replaced by Mg ions with charge ~+1.7 leading to a net charge of 0.8 electron per substitution). There are also small changes in the charges of the H and O atoms. Specifically, the basal oxygen atoms become more negatively charged in the MMTs compared to pyrophyllite making the basal surfaces in the MMTs more hydrophilic in nature. The H atoms of the hydroxyl groups of the MMTs also gain electron density compared to pyrophyllite making them less positive. This is accompanied by an increase in the O_hH bond lengths. The Bader analysis of the DFT charge densities gives similar charges for the Al atoms in the MMTs and in pyrophyllite. This is in contrast to the results of Huckel calculations, which gave less positively charged Al ions in the MMTs than in the pyrophyllite.[88] Finally, we note that our calculations give shorter O_aSi bond lengths and longer O_bSi bond lengths in the MMTs than in pyrophyllite. This trend was also found in the PW91 calculations of Minisini et al.[63] and can be understood in terms of the attraction between the interlayer cations and the basal oxygen atoms.

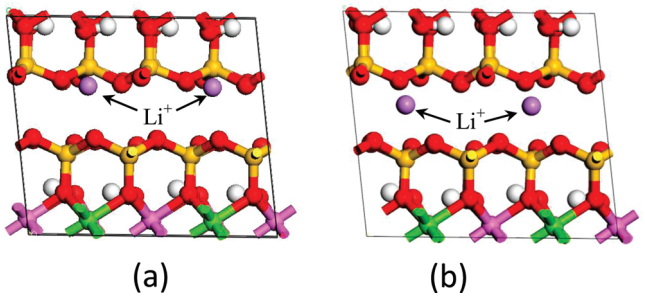

Figure 7. Structures corresponding to the double minima of the DFT-D2 potential energy curve shown in Figure 6: (a) the minimum at shorter *c* lattice parameter (9.33 Å) and (b) the minimum at the longer *c* lattice parameter (9.44 Å).

4. CONCLUSIONS

The structures of pyrophyllite and several montmorillonite minerals with various alkali and alkaline-earth interlayer cations were investigated using plane-wave density functional theory with the PBE functional, without dispersion corrections and with the DFT-D2 and vdW-TS dispersion correction schemes. For pyrophyllite, the dispersion-corrected PBE calculations closely reproduce the experimental structure, as well as the experimental value of the bulk modulus. For the montmorillonite minerals, our calculations reveal that the interlayer spacing correlates in a linear manner with the ionic radius of the intercalated cation. This correlation suggests that experimentally deduced interlayer distances reported for alkaline-earth MMTs should be taken with

Table 5. Differences between the Sum of Atomic Charges[a] for Each Atom Type[b] for Various MMT Systems from Those of Pyrophyllite

MMT	H_1	H_2	Al	Mg*[c]	O_{a1}	O_{a2}	O_{b1}	O_{b2}	O_{h1}	O_{h2}	Si_1	Si_2	M[d]
Li	−0.01	−0.12	0.01	−1.63	0.07	0.08	−0.10	−0.09	−0.02	0.09	−0.05	−0.05	1.80
Na	−0.07	−0.04	0.02	−1.63	0.05	0.08	−0.04	−0.08	0.05	0.00	−0.05	−0.06	1.75
K	−0.01	−0.10	0.01	−1.63	0.05	0.07	−0.11	−0.11	−0.02	0.07	−0.01	−0.03	1.82
Mg	−0.05	−0.08	0.02	−1.63	0.07	0.06	−0.05	−0.04	0.03	0.06	−0.06	−0.05	1.73
Ca	−0.06	−0.12	0.01	−1.62	0.04	0.09	−0.03	−0.02	0.04	0.11	−0.04	−0.06	1.66

[a] A negative (positive) sign indicates electron gain (loss) in going from pyrophyllite to the M-MMT. [b] The 1 and 2 in the subscripts refer respectively to sets 1 and 2 in Figure 1. [c] Mg* indicates the sum of difference in the charges of the two Mg "defect atoms" with respect to the corresponding Al atoms of pyrophyllite. [d] M gives the total charge on the interlayer cations.

dx.doi.org/10.1021/jp201277f |J. Phys. Chem. A 2011, 115, 9695–9703

caution because they show no apparent dependency on the chemical nature of the interlayer ion. For Li-montmorillonite, the DFT-D2 calculations predict two minima that differ primarily in the locations of the Li^+ counterions and the interlayer distances. Thus, upon compaction of the interlayer distance, the Li^+ ions change their positions and become closely coordinated with basal oxygen atoms in the tetrahedral holes of the clay layers. Such inclusion of Li^+ in the clay layers has been confirmed experimentally.

The inclusion of dispersion corrections in the DFT calculations leads to less flat potential energy curves for separating the layers, which, in turn, results in improved values of the bulk modulus. Dispersion interactions are also expected to be important for describing swelling and intercalation of water or carbon dioxide in clays. Thus, dispersion-corrected DFT calculations are well suited in providing information needed for understanding how swelling due to intercalation of water or CO_2 causes geo-mechanical stress, promoting development of cracks and fractures in porous media, information that is crucial in assessing clays for long-term geological storage of CO_2.

■ ACKNOWLEDGMENT

The authors are thankful to Drs. Evgeniy Myshakin, Vyacheslav Romanov, and Randall Cygan for fruitful discussions and comments on the manuscript. We acknowledge a grant of computer time at Pittsburgh Supercomputer Center and the use of computers at the University of Pittsburgh's Center for Simulation and Modeling. The research was performed under Contract DE-FE0004000, Subtask 4000.4.600.251.002.005.000.006, in support of the National Energy Technology Laboratory's Office of Research and Development. Reference in this report to any specific product, process, or service is to facilitate understanding and does not imply its endorsement or favoring by the United States Department of Energy.

■ REFERENCES

(1) Giese, R. F.; van Oss, C. J.; *Colloid and Surface Properties of Clays and Related Minerals*; Marcel Dekker: New York, 2002; Vol. 105.
(2) *Hydrous Phyllosilicates (Exclusive of Micas)*; Bailey, S. W., Ed.; Mineralogical Society of America: Washington, D.C., 1988; Vol. 19.
(3) Murray, H. H. *Appl. Clay Sci.* **2000**, *17*, 207.
(4) Sposito, G.; Skipper, N. T.; Sutton, R.; Park, S. H.; Soper, A. K.; Greathouse, J. A. *Proc. Natl. Acad. Sci. U.S.A.* **1999**, *96*, 3358.
(5) Hubbard, A. T. *Encyclopedia of Surface and Colloid Science*; CRC Press: Boca Raton, FL, 2002.
(6) Kato, M.; Usuki, A. *Polymer-Clay Nanocomposites*; Wiley: New York, 2000.
(7) Liu, Z.; Chen, K.; Yan, D. *Eur. Polym. J.* **2003**, *39*, 2359.
(8) Wan, C.; Qiao, X.; Zhang, Y.; Zhang, Y. *Polym. Test.* **2003**, *22*, 453.
(9) Zhang, Y. H.; Dang, Z. M.; Fu, S. Y.; Xin, J. H.; Deng, J. G.; Wu, J.; Yang, S.; Li, L. F.; Yan, Q. *Chem. Phys. Lett.* **2005**, *401*, 553.
(10) Qin, H.; Su, Q.; Zhang, S.; Zhao, B.; Yang, M. *Polymer* **2003**, *44*, 7533.
(11) Majumdar, D.; Blanton, T. N.; Schwark, D. W. *Appl. Clay Sci.* **2003**, *23*, 265.
(12) Chilingarian, G. V.; Vorabutr, P. *Drilling and Drilling Fluids*; Elsevier: New York, 1983.
(13) Bartelt-Hunt, S. L.; Smith, J. A.; Burns, S. E.; Rabideau, A. J. *J. Geotech. Geoenviron. Eng.* **2005**, *131*, 848.
(14) Dawson, G. W. *J. Hazard. Mater.* **1983**, *8*, 43.
(15) Koch, D. *Appl. Clay Sci.* **2002**, *21*, 1.
(16) Romanov, V. N.; Ackman, T. E.; Soong, Y.; Kleinman, R. L. *Environ. Sci. Technol.* **2009**, *43*, 561.
(17) Greenwell, H. C.; Jones, W.; Coveney, P. V.; Stackhouse, S. *J. Mater. Chem.* **2006**, *16*, 708.
(18) Petry, T. M.; Little, D. N. *J. Mater. Civil Eng.* **2002**, *14*, 447.
(19) Suquet, H.; de la Calle, C.; Pezerat, H. *Clays Clay Miner.* **1975**, *23*, 1.
(20) Guindy, N. M.; El-Akkad, T. M.; Flex, N. S.; El-Massry, S. R.; Nashed, S. *Thermochim. Acta* **1985**, *88*, 369.
(21) Fu, M. H.; Zhang, Z. Z.; Low, P. F. *Clays Clay Miner.* **1990**, *38*, 485.
(22) Slade, P. G.; Quirk, J. P.; Norrish, K. *Clays Clay Miner.* **1991**, *39*, 234.
(23) Sato, T.; Watanabe, T.; Otsuka, R. *Clays Clay Miner.* **1992**, *40*, 103.
(24) Berend, I.; Cases, J. M.; Francois, M.; Uriot, J. P.; Michot, L.; Masion, A.; Thomas, F. *Clays Clay Miner.* **1995**, *43*, 324.
(25) Cases, J. M.; Berend, I.; Francois, M.; Uriot, J. P.; Michot, L. J.; Thomas, F. *Clays Clay Miner.* **1997**, *45*, 8.
(26) Cuadros, J. *Am. J. Sci.* **1997**, *297*, 829.
(27) Dios Cancela, G.; Huertas, F. J.; Romero Taboada, E.; Sánchez-Rasero, F.; Hernández Laguna, A. *J. Colloid Interface Sci.* **1997**, *185*, 343.
(28) Zabat, M.; Van Damme, H. *Clay Miner.* **2000**, *35*, 357.
(29) Bray, H. J.; Redfern, S. A. T. *Phys. Chem. Miner.* **1999**, *26*, 591.
(30) Ferrage, E.; Lanson, B.; Sakharov, B. A.; Drits, V. A. *Am. Mineral.* **2005**, *90*, 1358.
(31) Ferrage, E.; Lanson, B.; Sakharov, B. A.; Geoffroy, N.; Jacquot, E.; Drits, V. A. *Am. Mineral.* **2007**, *92*, 1731.
(32) Ferrage, E.; Kirk, C. A.; Cressey, G.; Cuadros, J. *Am. Mineral.* **2007**, *92*, 994.
(33) Abramova, E.; Lapides, I.; Yariv, S. *J. Therm. Anal. Calorim.* **2007**, *90*, 99.
(34) Cygan, R. T.; Liang, J. J.; Kalinichev, A. G. *J. Phys. Chem. B* **2004**, *108*, 1255.
(35) Heinz, H.; Koerner, H.; Anderson, K. L.; Vaia, R. A.; Farmer, B. L. *Chem. Mater.* **2005**, *17*, 5658.
(36) Ugliengo, P.; Zicovich-Wilson, C. M.; Tosoni, S.; Civalleri, B. *J. Mater. Chem.* **2009**, *19*, 2564.
(37) Teppen, B. J.; Rasmussen, K.; Bertsch, P. M.; Miller, D. M.; Schafer, L. *J. Phys. Chem. B* **1997**, *101*, 1579.
(38) Bougeard, D.; Smirnov, K. S.; Geidel, E. *J. Phys. Chem. B* **2000**, *104*, 9210.
(39) Sainz-Diaz, C. I.; Hernández-Laguna, A.; Dove, M. T. *Phys. Chem. Miner.* **2001**, *28*, 130.
(40) Skipper, N. T.; Refson, K.; McConnell, J. D. C. *J. Chem. Phys.* **1991**, *94*, 7434.
(41) Heinz, H.; Castelijns, H. J.; Suter, U. W. *J. Am. Chem. Soc.* **2003**, *125*, 9500.
(42) Ermoshin, V. A.; Smirnov, K. S.; Bougeard, D. *Surf. Sci.* **1996**, *368*, 147.
(43) Ermoshin, V. A.; Smirnov, K. S.; Bougeard, D. *Chem. Phys.* **1996**, *209*, 41.
(44) Hill, J. R.; Sauer, J. *J. Phys. Chem.* **1995**, *99*, 9536.
(45) Zartman, G. D.; Liu, H.; Akdim, B.; Pachter, R.; Heinz, H. *J. Phys. Chem. C* **2010**, *114*, 1763.
(46) Sainz-Diaz, C. I.; Timon, V.; Botella, V.; Artacho, E.; Hernandez-Laguna, A. *Am. Mineral.* **2002**, *87*, 958.
(47) Timon, V.; Sainz-Diaz, C. I.; Botella, V.; Hernandez-Laguna, A. *Am. Mineral.* **2003**, *88*, 1788.
(48) Hernández-Laguna, A.; Escamilla-Roa, E.; Timón, V.; Dove, M.; Sainz-Díaz, C. *Phys. Chem. Miner.* **2006**, *33*, 655.
(49) Chatterjee, A.; Ebina, T.; Onodera, Y.; Mizukami, F. *J. Chem. Phys.* **2004**, *120*, 3414.
(50) Berghout, A.; Tunega, D.; Zaoui, A. *Clays Clay Miner.* **2010**, *58*, 174.
(51) Mounet, N.; Marzari, N. *Phys. Rev. B* **2005**, *71*, 205214.
(52) Ooi, N.; Rairkar, A.; Adams, J. B. *Carbon* **2006**, *44*, 231.
(53) Grimme, S. *J. Comput. Chem.* **2004**, *25*, 1463.
(54) Grimme, S. *J. Comput. Chem.* **2006**, *27*, 1787.

(55) Grimme, S.; Antony, J.; Ehrlich, S.; Krieg, H. *J. Chem. Phys.* **2010**, *132*, 154104.
(56) Lee, K.; Murray, E. D.; Kong, L.; Lundqvist, B. I.; Langreth, D. C. *Phys. Rev. B* **2010**, *82*, 081101.
(57) Dion, M.; Rydberg, H.; Schröder, E.; Langreth, D. C.; Lundqvist, B. I. *Phys. Rev. Lett.* **2004**, *92*, 246401.
(58) Andersson, Y.; Langreth, D. C.; Lundqvist, B. I. *Phys. Rev. Lett.* **1996**, *76*, 102.
(59) von Lilienfeld, O. A.; Tavernelli, I.; Rothlisberger, U.; Sebastiani, D. *Phys. Rev. Lett.* **2004**, *93*, 153004.
(60) Tavernelli, I.; Lin, I. C.; Rothlisberger, U. *Phys. Rev. B* **2009**, *79*, 045106.
(61) Tkatchenko, A.; Scheffler, M. *Phys. Rev. Lett.* **2009**, *102*, 073005.
(62) Tunega, D.; Goodman, B. A.; Haberhauer, G.; Reichenauer, T. G.; Gerzabek, M. H.; Lischka, H. *Clays Clay Miner.* **2007**, *55*, 220.
(63) Minisini, B.; Tsobnang, F. *Appl. Surf. Sci.* **2005**, *242*, 21.
(64) Kresse, G.; Hafner, J. *Phys. Rev. B* **1993**, *47*, 558.
(65) Kresse, G.; Furthmuller, J. *Phys. Rev. B* **1996**, *54*, 11169.
(66) Blochl, P. E. *Phys. Rev. B* **1994**, *50*, 17953.
(67) Perdew, J. P.; Burke, K.; Ernzerhof, M. *Phys. Rev. Lett.* **1996**, *77*, 3865.
(68) Bučko, T.; Hafner, J.; Lebègue, S.; Angyàn, J. G. *J. Phys. Chem. A* **2010**, *114*, 11814.
(69) Voora, V.; Al-Saidi, W. A.; Jordan, K. D. 2011, manuscript to be submitted for publication.
(70) Monkhorst, H. J.; Pack, J. D. *Phys. Rev. B* **1976**, *13*, 5188.
(71) Francis, G. P.; Payne, M. C. *J. Phys.: Condens. Matter* **1990**, *2*, 4395.
(72) Birch, F. *Phys. Rev.* **1947**, *71*, 809.
(73) Bader, R. F. W. *Chem. Rev.* **1991**, *91*, 893.
(74) Henkelman, G.; Arnaldsson, A.; Jónsson, H. *Comput. Mater. Sci.* **2006**, *36*, 354.
(75) Hirshfeld, F. L. *Theor. Chim. Acta* **1977**, *44*, 129.
(76) Lee, J. H.; Guggenheim, S. *Am. Mineral.* **1981**, *66*, 350.
(77) Refson, K.; Park, S. H.; Sposito, G. *J. Phys. Chem. B* **2003**, *107*, 13376.
(78) Craig, M. S.; Warren, M. C.; Dove, M. T.; Gale, J. D.; Sanchez-Portal, D.; Ordejon, P.; Soler, J. M.; Artacho, E. *Phys. Chem. Miner.* **2004**, *31*, 12.
(79) Wardle, R. B., G. W. *Am. Mineral.* **1972**, *57*, 732.
(80) Pawley, A. R.; Clark, S. M.; Chinnery, N. J. *Am. Mineral.* **2002**, *87*, 1172.
(81) Becke, A. D. *Phys. Rev. A* **1988**, *38*, 3098.
(82) Perdew, J. P.; Wang, Y. *Phys. Rev. B* **1992**, *45*, 13244.
(83) Shannon, R. *Acta Crystallogr., Sect. A* **1976**, *32*, 751.
(84) Boek, E. S.; Coveney, P. V.; Skipper, N. T. *Langmuir* **1995**, *11*, 4629.
(85) Tambach, T. J.; Bolhuis, P. G.; Smit, B. *Angew. Chem.* **2004**, *116*, 2704.
(86) Stackhouse, S.; Coveney, P. V. *J. Phys. Chem. B* **2002**, *106*, 12470.
(87) Boulet, P.; Greenwell, H. C.; Stackhouse, S.; Coveney, P. V. *THEOCHEM* **2006**, *762*, 33.
(88) Bleam, W. F.; Hoffmann, R. *Inorg. Chem.* **1988**, *27*, 3180.